

Photon asymmetries in $nd \rightarrow {}^3H\gamma$ using EFT($\not{\pi}$) approach

M. Moeini Arani* and S. Bayegan†

Department of Physics, University of Tehran, P.O.Box 14395-547, Tehran, Iran

(Dated: May 14, 2021)

Abstract

The parity-violating Lagrangian of the weak nucleon-nucleon (NN) interaction in the pionless effective field theory (EFT($\not{\pi}$)) approach contains five independent unknown low-energy coupling constants (LECs). The photon asymmetry with respect to neutron polarization in $np \rightarrow d\gamma$ A_γ^{np} , the circular polarization of outgoing photon in $np \rightarrow d\gamma$ P_γ^{np} , the neutron spin rotation in hydrogen $\frac{1}{\rho} \frac{d\phi^{np}}{dl}$, the neutron spin rotation in deuterium $\frac{1}{\rho} \frac{d\phi^{nd}}{dl}$ and the circular polarization of γ -emission in $nd \rightarrow {}^3H\gamma$ P_γ^{nd} are the parity-violating observables which have been recently calculated in terms of parity-violating LECs in the EFT($\not{\pi}$) framework. We obtain the LECs by matching the parity-violating observables to the Desplanques, Donoghue, and Holstein (DDH) best value estimates. Then, we evaluate photon asymmetry with respect to the neutron polarization a_γ^{nd} and the photon asymmetry in relation to deuteron polarization A_γ^{nd} in $nd \rightarrow {}^3H\gamma$ process. We finally compare our EFT($\not{\pi}$) photon asymmetries results with the experimental values and the previous calculations based on the DDH model.

PACS numbers:

*m.moeini.a@khayam.ut.ac.ir (corresponding author)

†bayegan@khayam.ut.ac.ir

I. INTRODUCTION

The theoretical analyses of the hadronic parity violation in few-nucleon systems were introduced by Danilov [1] and Desplanques and Missimer [2] for the first time. The analysis of parity-violating (PV) couplings in a meson-exchange model was then developed by Desplanques, Donoghue, and Holstein (DDH) [3]. At low energies, the DDH potential is dominated by the exchange of light mesons as a sign of the long-distance physics. The inclusion of heavy ρ and ω mesons in DDH model point out the short-distance physics. With these model assumptions, the DDH potential has been widely used to calculate PV observables in terms of PV meson-exchange couplings for different few-body systems [4].

The idea of the effective field theory (EFT) and its application in low-energy parity violation is principally based on the fact that the long-distance physics should be independent of the details of the short-distance effects. Therefore, the PV transition amplitudes with no reference to the description of the short-distance effects are appropriate in order to determine the PV observables.

Recently, the PV Lagrangian of the weak nucleon-nucleon (NN) interaction of the pionless effective field theory (EFT(\hbar)) with five independent unknown low-energy coupling constants (LECs) has been incorporated to evaluate the following PV observables in terms of PV LECs in a unified EFT(\hbar) framework. The photon asymmetry with respect to neutron polarization A_γ^{np} and the circular polarization of outgoing photon P_γ^{np} in $np \rightarrow d\gamma$ were calculated by Schindler *et al.* [5]. The neutron spin rotation in hydrogen $\frac{1}{\rho} \frac{d\phi^{np}}{dt}$ and the neutron spin rotation in deuterium $\frac{1}{\rho} \frac{d\phi^{nd}}{dt}$ were evaluated by Griesshammer *et al.* in [6]. Also, the circular polarization of γ -emission in $nd \rightarrow {}^3H\gamma$ P_γ^{nd} was calculated by Arani and Bayegan in [7].

The older experimental data for A_γ^{np} are $(-0.6 \pm 0.21) \times 10^{-7}$ [8] and $(-0.15 \pm 0.47) \times 10^{-7}$ [9]. The newer measurement of A_γ^{np} has been reported with a statistical precision of 5×10^{-9} and with negligible systematic error [10]. The only available data for P_γ^{np} is $(1.8 \pm 1.8) \times 10^{-7}$ [11]. At present, there are no experimental data on the neutron-proton (np) and the neutron-deuteron (nd) spin rotations. The experimental data for P_γ^{nd} has not been reported to this point. In order to determine PV LECs, we need to increase the accuracy of existing measurement and to plan new experiments for measuring the neutron spin rotation on a variety of targets and the circular photon polarization for unpolarized beam and target [4].

The lack of experimental values for the PV observables are the main obstacle to determine the PV LECs. Therefore, in this paper, we intend to obtain the five independent PV LECs by matching the five EFT(\hbar) relations for PV observables A_γ^{np} , P_γ^{np} , $\frac{1}{\rho} \frac{d\phi^{np}}{dl}$, $\frac{1}{\rho} \frac{d\phi^{nd}}{dl}$ and P_γ^{nd} to DDH "best" values estimates for these observables. The determination of the PV LECs provides the calculation of the asymmetry of the outgoing photon with respect to the neutron a_γ^{nd} , and the deuteron A_γ^{nd} , polarizations. The photon asymmetries results are then compared with the experimental values and the previous calculations based on the DDH model.

The reminder of this paper is organized as follows. In Sect.II we briefly review the leading-order (LO) Lagrangians of the strong two- and three-nucleon, the weak NN and the electromagnetic interactions. In Sect.III, we introduce the parity-conserving (PC) and parity-violating amplitudes of $nd \rightarrow {}^3H\gamma$ and calculate the P_γ^{nd} , a_γ^{nd} and A_γ^{nd} observables in $nd \rightarrow {}^3H\gamma$ process in terms of PV LECs. In Sect.IV the EFT(\hbar) results of A_γ^{np} , P_γ^{np} , $\frac{1}{\rho} \frac{d\phi^{np}}{dl}$ and $\frac{1}{\rho} \frac{d\phi^{nd}}{dl}$ observables in terms of the PV low-energy constants are presented and used for obtaining PV LECs. Sect.V contains our EFT(\hbar) results for a_γ^{nd} and A_γ^{nd} which are evaluated by the determined PV LECs. The conclusion and outlook are expressed in Sect.VI.

II. LAGRANGIAN

In this section, we introduce Lagrangians of the strong, weak and electromagnetic interactions in the three-body system at the lowest order. In the EFT approach with the Z-parametrization structure, the strong two- and three-nucleon interactions are presented by [12, 13]

$$\begin{aligned} \mathcal{L}^{PC} = & N^\dagger \left(iD_0 + \frac{\vec{D}^2}{2m_N} \right) N + d_s^{A\dagger} \left[\Delta_s - c_{0s} \left(iD_0 + \frac{\vec{D}^2}{4m_N} + \frac{\gamma_s^2}{m_N} \right) \right] d_s^A \\ & + d_t^{i\dagger} \left[\Delta_t - c_{0t} \left(iD_0 + \frac{\vec{D}^2}{4m_N} + \frac{\gamma_t^2}{m_N} \right) \right] d_t^i - y \left(d_s^{A\dagger} (N^T P^A N) + d_t^{i\dagger} (N^T P^i N) + h.c. \right) \\ & + \frac{m_N y^2 H_0(\Lambda)}{3\Lambda^2} N^\dagger \left((d_t^i \sigma_i)^\dagger (d_t^j \sigma_j) - [(d_t^i \sigma_i)^\dagger (d_s^A \tau_A) + h.c.] + (d_s^A \tau_A)^\dagger (d_s^B \tau_B) \right) N + \dots \quad (1) \end{aligned}$$

where N is the nucleon iso-doublet and the auxiliary fields $d_s^{A(B)}$ and $d_t^{i(j)}$ carry the quantum numbers of 1S_0 di-nucleon and the deuteron, respectively. $D_\mu = \partial_\mu + ie \frac{1+\tau_3}{2} A_\mu$ is the nucleon covariant derivative. The operators P^i and P^A project NN system into the triplet and singlet channels, respectively. $\tau_{A/B}$ ($\sigma_{i/j}$) are isospin (spin) pauli matrices with $A, B = 1, 2, 3$ ($i, j = 1, 2, 3$) as iso-triplet (vector) indices. m_N is the nucleon mass and the three-nucleon

interaction at the leading order is $H_0(\Lambda)$ with cut-off Λ . The parameters of the Lagrangian in Eq.(1) are fixed using Z-parametrization [13]. So, dibaryon-nucleon-nucleon (dNN) coupling constant is chosen as $y^2 = \frac{4\pi}{m_N}$ and the LO parameters $\Delta_{s/t}$ are obtained from the poles of the NN S-wave scattering amplitude at $i\gamma_{s/t}$ where $\gamma_s = \frac{1}{a_s}$ with a_s as the scattering length in 1S_0 state and γ_t is the binding momentum of the deuteron.

The Lagrangian

$$\begin{aligned}
\mathcal{L}_{PV} = & - \left[g^{(^3S_1-^1P_1)} d_t^{i\dagger} N^T i \left(\overleftarrow{\nabla} \sigma_2 \tau_2 - \sigma_2 \tau_2 \overrightarrow{\nabla} \right)_i N \right. \\
& + g_{(\Delta I=0)}^{(^1S_0-^3P_0)} d_s^{A\dagger} N^T i \left(\overleftarrow{\nabla} \sigma_2 \sigma_i \tau_2 \tau_A - \sigma_2 \sigma_i \tau_2 \tau_A \overrightarrow{\nabla} \right)_i N \\
& + g_{(\Delta I=1)}^{(^1S_0-^3P_0)} \epsilon^{3AB} d_s^{A\dagger} N^T i \left(\overleftarrow{\nabla} \sigma_2 \sigma_i \tau_2 \tau^B - \sigma_2 \sigma_i \tau_2 \tau^B \overrightarrow{\nabla} \right)_i N \\
& + g_{(\Delta I=2)}^{(^1S_0-^3P_0)} \mathcal{I}^{AB} d_s^{A\dagger} N^T i \left(\overleftarrow{\nabla} \sigma_2 \sigma_i \tau_2 \tau^B - \sigma_2 \sigma_i \tau_2 \tau^B \overrightarrow{\nabla} \right)_i N \\
& \left. + g^{(^3S_1-^3P_1)} \epsilon^{ijk} d_t^{i\dagger} N^T \left(\overleftarrow{\nabla} \sigma_2 \sigma^k \tau_2 \tau_3 - \sigma_2 \sigma^k \tau_2 \tau_3 \overrightarrow{\nabla} \right)^j N \right] \\
& + h.c. + \dots
\end{aligned} \tag{2}$$

introduces the weak NN interactions with the dibaryon formalism at the very-low-energy regime. The Lagrangian in Eq.(2) is constructed by considering five transitions which mix the S-P partial waves. In the above equation, the weak dNN coupling constant for the PV NN transition between \bar{X} and \bar{Y} partial waves is depicted by $g^{(\bar{X}-\bar{Y})}$. ΔI represents the isospin change in the PV vertex and

$$\mathcal{I} = \begin{pmatrix} 1 & 0 & 0 \\ 0 & 1 & 0 \\ 0 & 0 & -2 \end{pmatrix}. \tag{3}$$

With considering the PV NN Lagrangian introduced in Eq.(2), the parity-violating observables in the three-body systems are cutoff independent at the leading order and next-to-leading order (NLO) [7, 14]. So, the parity-violating three-nucleon interaction (PV 3NI) is not participated in the three-nucleon systems at LO and NLO in EFT($\not{\pi}$).

At the leading order, the electromagnetic interactions are introduced by the Lagrangian

$$\mathcal{L}^{EM} = \frac{e}{2m_N} \left[N^\dagger (k_0 + k_1 \tau^3) \vec{\sigma} \cdot \vec{B} N + N^\dagger \frac{(1 + \tau_3)}{2} (\vec{P} + \vec{P}') \cdot \vec{\varepsilon}_\gamma^* N \right], \tag{4}$$

where the first and second terms indicate the M1 and E1 interactions of a photon with a single nucleon, respectively. k_0 and k_1 are the isoscalar and isovector nucleon magnetic moments.

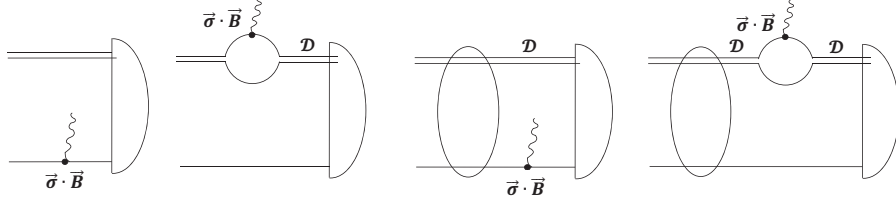


FIG. 1: The leading-order diagrams which contribute to PC (M1) amplitude of $nd \rightarrow {}^3H\gamma$. Single, double and wavy lines denote a nucleon, a dibaryon auxiliary field with the propagator matrix of $\mathcal{D} = \text{diag}(D_t, D_s)$ and a photon, respectively. Dashed oval and dashed half-oval indicate Nd scattering amplitude at LO which is shown in Fig.3 of Appendix and the formation of triton (the normalized triton wave function).

e , \vec{B} , \vec{P} (\vec{P}') and $\vec{\varepsilon}_\gamma$ denote the electric charge, the magnetic field, the incoming (outgoing) nucleon momentum and the 3-vector polarization of the produced photon, respectively.

III. $nd \rightarrow {}^3H\gamma$ SYSTEM

A. PC amplitude of $nd \rightarrow {}^3H\gamma$ process

The leading-order diagrams which contribute to the PC amplitude of $nd \rightarrow {}^3H\gamma$ process are shown in Fig.1. In the cluster-configuration space the propagators of two intermediate dibaryon auxiliary fields d_t^i and d_s^A at LO are presented by $\mathcal{D} = \text{diag}(D_t, D_s)$ where $D_{t(s)}$ is

$$D_{t(s)}(q_0, q) = \frac{1}{\gamma_{t(s)} - \sqrt{\frac{q^2}{4} - m_N q_0} - i\varepsilon}. \quad (5)$$

The PC nucleon-deuteron (Nd) scattering (the dashed oval) and the normalized triton wave function (the dashed half-oval) in Fig.1 are obtained by solving the Faddeev equation and the homogenous part of the Faddeev equation introduced in Fig.3 of Appendix, respectively [7, 13].

In order to compute the LO PC amplitude of $nd \rightarrow {}^3H\gamma$ process for two M1 transitions corresponding to the initial ${}^2S_{\frac{1}{2}}$ and ${}^4S_{\frac{3}{2}}$ states, we use the Lagrangian of Eq.(1) for the strong interaction and the first terms of Eq.(4) for the M1 interaction. In the cluster-configuration space, one can be able to write the contribution of the diagrams in Fig.1 for

both possible magnetic transitions with initial doublet and quartet channels as

$$\mathcal{M}^{PC} = \mathcal{W}^{PC}(^2S_{\frac{1}{2}})Y^{PC}(^2S_{\frac{1}{2}}) + \mathcal{W}^{PC}(^4S_{\frac{3}{2}})Y^{PC}(^4S_{\frac{3}{2}}), \quad (6)$$

where

$$\begin{aligned} Y^{PC}(^2S_{\frac{1}{2}}) &= t^\dagger (i\vec{\varepsilon}_d \cdot \vec{\varepsilon}_\gamma^* \times \vec{q} + \vec{\sigma} \times \vec{\varepsilon}_d \cdot \vec{\varepsilon}_\gamma^* \times \vec{q})N, \\ Y^{PC}(^4S_{\frac{3}{2}}) &= t^\dagger (2i\vec{\varepsilon}_d \cdot \vec{\varepsilon}_\gamma^* \times \vec{q} - \vec{\sigma} \times \vec{\varepsilon}_d \cdot \vec{\varepsilon}_\gamma^* \times \vec{q})N. \end{aligned} \quad (7)$$

t , $\vec{\varepsilon}_d$ and \vec{q} are the final 3H (or 3He) field, the 3-vector polarization of the deuteron and the unit vector along the 3-momentum of the photons, respectively. In Eq.(6), $\mathcal{W}^{PC}(X)$ with $X = ^2S_{\frac{1}{2}}, ^4S_{\frac{3}{2}}$ is a 2×1 matrix which is given in the cluster-configuration space by

$$\mathcal{W}^{PC}(X) = \begin{pmatrix} \mathcal{W}_{nd_t \rightarrow ^3H(nd_t)\gamma}^{PC}(X) \\ \mathcal{W}_{nd_t \rightarrow ^3H(nd_s)\gamma}^{PC}(X) \end{pmatrix} \quad (8)$$

where $\mathcal{W}_{nd_t \rightarrow ^3H(nd_t(s))\gamma}^{PC}(X)$ denotes the contribution of all diagrams in Fig.1 for PC $nd_t \rightarrow ^3H(nd_t(s))\gamma$ transition. $^3H_{(nd_t)}$ and $^3H_{(nd_s)}$ represent the final triton components which are made from the final doublet nd_t (nucleon and triplet dibaryon) and nd_s (nucleon and singlet dibaryon) cases, respectively.

The results of $\mathcal{W}^{PC}(X)$ ($X = ^2S_{\frac{1}{2}}, ^4S_{\frac{3}{2}}$) are used for the evaluation of the PV observables in Sect.III C.

B. PV amplitude of $nd \rightarrow ^3H\gamma$ process

In the next step, we explain briefly our EFT(\mathcal{F}) results for the PV (E1) amplitude of $nd \rightarrow ^3H\gamma$ process based on the procedure presented in ref.[7].

The Lagrangians in Eqs.(2) and (4) are used for the weak and E1 interactions, respectively. By working in the coulomb gauge, the spin structure of the PV (E1) amplitude of $nd \rightarrow ^3H\gamma$ process can be written as two orthogonal terms,

$$i(t^\dagger \sigma_a N) (\vec{\varepsilon}_d \times \vec{\varepsilon}_\gamma^*)_a, \quad (t^\dagger N) (\vec{\varepsilon}_d \cdot \vec{\varepsilon}_\gamma^*). \quad (9)$$

Similar to the PC subsection, the contribution of E1 transition which is the sum of both contributions corresponding to the incoming doublet ($X = ^2S_{\frac{1}{2}}$) and quartet ($X = ^4S_{\frac{3}{2}}$) channels can be written as

$$\mathcal{M}^{PV} = \mathcal{W}^{PV}(^2S_{\frac{1}{2}})Y^{PV}(^2S_{\frac{1}{2}}) + \mathcal{W}^{PV}(^4S_{\frac{3}{2}})Y^{PV}(^4S_{\frac{3}{2}}), \quad (10)$$

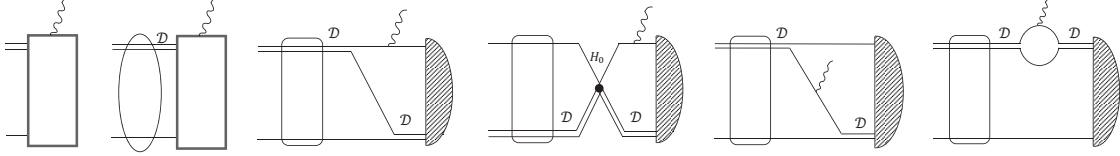


FIG. 2: The diagrams of the PV $nd \rightarrow {}^3H\gamma$ process at LO. The photon-nucleon-nucleon vertex represents one-body current for E1 interaction. H_0 is three-body interaction which renormalizes the Nd scattering amplitude at LO. The dashed rectangular and the box with the wavy line are the PV Nd scattering amplitude and the sum of several diagrams which participate in the PV $nd \rightarrow {}^3H\gamma$ amplitude at LO, respectively (for more detail see Appendix). All notations are the same as the previous figures.

with

$$\begin{aligned}
 Y^{PV}({}^2S_{\frac{1}{2}}) &= t^\dagger (\vec{\varepsilon}_d \cdot \vec{\varepsilon}_\gamma^* + i\vec{\sigma} \cdot \vec{\varepsilon}_d \times \vec{\varepsilon}_\gamma^*) N, \\
 Y^{PV}({}^4S_{\frac{3}{2}}) &= t^\dagger (\vec{\varepsilon}_d \cdot \vec{\varepsilon}_\gamma^* + i\vec{\sigma} \cdot \vec{\varepsilon}_d \times \vec{\varepsilon}_\gamma^*) N,
 \end{aligned}
 \tag{11}$$

where $\mathcal{W}^{PV}(X) = \begin{pmatrix} \mathcal{W}_{nd_t \rightarrow {}^3H_{(nd_t)}\gamma}^{PV}(X) \\ \mathcal{W}_{nd_t \rightarrow {}^3H_{(nd_s)}\gamma}^{PV}(X) \end{pmatrix}$ with $\mathcal{W}_{nd_t \rightarrow {}^3H_{(nd_t(s))}\gamma}^{PV}(X)$ denotes the contribution of PV $nd_t \rightarrow {}^3H_{(nd_t(s))}\gamma$ amplitude for E1 transition in the cluster-configuration space with the incoming X partial wave.

All possible diagrams which consider the weak interaction effects in $nd \rightarrow {}^3H\gamma$ process at LO are depicted in Fig.2. The dashed rectangular with solid line around it denotes the LO PV Nd scattering amplitude which is recently calculated by Griesshammer *et al.*, with EFT approach [6]. The box with the wavy line is the sum of several diagrams which contribute in the amplitude of PV radiative capture of neutron by deuteron. All diagrams which make contributions of the dashed rectangular (PV Nd scattering amplitude) and the box with the wavy line in Fig.2 are presented briefly in Appendix.

With respect to the diagrams introduced in Fig.2, we obtain the PV amplitude of neutron radiative capture by deuteron for incoming X ($X = {}^2S_{\frac{1}{2}}, {}^4S_{\frac{3}{2}}$) channel in terms of the PV

TABLE I: Results of $a_x(\bar{X} - \bar{Y})$ for the different incoming and outgoing partial waves with $\Lambda = 700$ MeV. $a_{2S_{\frac{1}{2}}}(\bar{X} - \bar{Y})$ and $a_{4S_{\frac{3}{2}}}(\bar{X} - \bar{Y})$ results are in 10^{-2} MeV^{-1} and 10^{-4} MeV^{-1} units, respectively.

X	$a_x(^3S_1 -^1P_1)$	$a_x(^1S_0 -^3P_0, \Delta I = 0)$	$a_x(^1S_0 -^3P_0, \Delta I = 1)$	$a_x(^3S_1 -^3P_1)$
$^2S_{\frac{1}{2}}$	$\begin{pmatrix} -0.75 \\ 0.55 \end{pmatrix}$	$\begin{pmatrix} 1.24 \\ -0.80 \end{pmatrix}$	$\begin{pmatrix} -0.73 \\ 0.49 \end{pmatrix}$	$\begin{pmatrix} 2.35 \\ -1.16 \end{pmatrix}$
$^4S_{\frac{3}{2}}$	$\begin{pmatrix} 7.62 \\ -3.10 \end{pmatrix}$	$\begin{pmatrix} 3.32 \\ -0.63 \end{pmatrix}$	$\begin{pmatrix} 0.42 \\ -0.26 \end{pmatrix}$	$\begin{pmatrix} -28.87 \\ 7.93 \end{pmatrix}$

TABLE II: Results of $Abs[1 - \frac{a_x(\bar{X} - \bar{Y}) \text{ at } \Lambda=400 \text{ MeV}}{a_x(\bar{X} - \bar{Y}) \text{ at } \Lambda=700 \text{ MeV}}]$ for the different incoming and outgoing partial waves.

X	$(^3S_1 -^1P_1)$	$(^1S_0 -^3P_0, \Delta I = 0)$	$(^1S_0 -^3P_0, \Delta I = 1)$	$(^3S_1 -^3P_1)$
$^2S_{\frac{1}{2}}$	$\begin{pmatrix} 0.0477 \\ 0.0978 \end{pmatrix}$	$\begin{pmatrix} 0.0358 \\ 0.0917 \end{pmatrix}$	$\begin{pmatrix} 0.0526 \\ 0.1098 \end{pmatrix}$	$\begin{pmatrix} 0.0212 \\ 0.0591 \end{pmatrix}$
$^4S_{\frac{3}{2}}$	$\begin{pmatrix} 0.0300 \\ 0.1100 \end{pmatrix}$	$\begin{pmatrix} 0.1402 \\ 0.1474 \end{pmatrix}$	$\begin{pmatrix} 0.1057 \\ 0.0888 \end{pmatrix}$	$\begin{pmatrix} 0.0021 \\ 0.0350 \end{pmatrix}$

LECs which have been introduced in Eq.(2),

$$\begin{aligned}
\mathcal{W}^{PV}(X) = & a_x(^3S_1 -^1P_1) g^{(^3S_1 -^1P_1)} \\
& + a_x(^1S_0 -^3P_0, \Delta I = 0) g_{(\Delta I=0)}^{(^1S_0 -^3P_0)} \\
& + a_x(^1S_0 -^3P_0, \Delta I = 1) g_{(\Delta I=1)}^{(^1S_0 -^3P_0)} \\
& + a_x(^3S_1 -^3P_1) g^{(^3S_1 -^3P_1)}.
\end{aligned} \tag{12}$$

In Eq.(12), the $a_x(\bar{X} - \bar{Y})$ is a 2×1 coefficient matrix of $g^{(\bar{X} - \bar{Y})}$ for incoming X partial wave. We evaluate numerically the value of the $a_x(\bar{X} - \bar{Y})$ coefficient matrix for $X = ^2S_{\frac{1}{2}}, ^4S_{\frac{3}{2}}$ with $\Lambda = 700 \text{ MeV}$. Our results for $a_x(\bar{X} - \bar{Y})$ coefficient matrix are shown in Table I. The leading-order $\mathcal{W}^{PV}(X)$ does not contain $g_{(\Delta I=2)}^{(^1S_0 -^3P_0)}$ term because the Nd system is an iso-doublet and PV coupling $g_{(\Delta I=2)}^{(^1S_0 -^3P_0)}$ cannot contribute.

The cutoff variation of the $a_x(\bar{X} - \bar{Y})$ results are investigated by calculating the $Abs[1 -$

$\frac{a_x(\bar{X}-\bar{Y}) \text{ at } \Lambda=400 \text{ MeV}}{a_x(X-Y) \text{ at } \Lambda=700 \text{ MeV}}$] for the different incoming and outgoing partial waves. Our results for the cutoff variation of the coefficient matrix $a_x(\bar{X}-\bar{Y})$ are shown in Table II. These results indicate that the cutoff dependence is small at the leading order. This small variation can be removed with the consideration of the higher-order corrections. The negligible cutoff variation of the PV amplitude of $nd \rightarrow {}^3H\gamma$ process represents that we do not need the PV 3NI at LO because the PV amplitude of the neutron radiative capture by deuteron is properly renormalized.

In the next sections, we concentrate on finding the PV observables in $nd \rightarrow {}^3H\gamma$ process with using Eq.(12) and the results in the Table I.

C. PV observables in $nd \rightarrow {}^3H\gamma$ process in terms of PV LECs

We have briefly clarified the PC and PV amplitudes of $nd \rightarrow {}^3H\gamma$ process, we then proceed by introducing the PV observables in $nd \rightarrow {}^3H\gamma$. The circular polarization of outgoing photon P_γ^{nd} , the photon asymmetry with respect to the neutron polarization a_γ^{nd} and the asymmetry of photon in relation to the deuteron polarization A_γ^{nd} are three PV observables in $nd \rightarrow {}^3H\gamma$. We discuss about the calculation of these observables in the following.

1. Photon circular polarization in $nd \rightarrow {}^3H\gamma$

The PV polarization of photon is defined by

$$P_\gamma = \frac{\sigma_+ - \sigma_-}{\sigma_+ + \sigma_-}, \quad (13)$$

where σ_+ and σ_- are the capture cross section for photons with positive and negative helicity, respectively.

From Eq.(13), we can write the PV polarization of photon in $nd \rightarrow {}^3H\gamma$ as

$$P_\gamma^{nd} = 2 \frac{\text{Re} \left[\mathcal{W}^{PC\dagger}(2S_{\frac{1}{2}}) \mathcal{W}^{PV}(2S_{\frac{1}{2}}) + \mathcal{W}^{PC\dagger}(4S_{\frac{3}{2}}) \mathcal{W}^{PV}(4S_{\frac{3}{2}}) \right]}{|\mathcal{W}^{PC}(2S_{\frac{1}{2}})|^2 + |\mathcal{W}^{PC}(4S_{\frac{3}{2}})|^2}, \quad (14)$$

where $\mathcal{W}^{PC}(X)$ and $\mathcal{W}^{PV}(X)$ are the PC (M1) and PV (E1) amplitudes of $nd \rightarrow {}^3H\gamma$ process which are introduced and evaluated in Sects.III A and III B, respectively.

We insert the results of the $\mathcal{W}^{PC}(X)$ and $\mathcal{W}^{PV}(X)$ for both incoming doublet and quartet channels in Eq.(14). The calculated result of P_γ^{nd} in terms of PV LECs is given by

$$\begin{aligned}
P_\gamma^{nd} = & \left[0.26 g^{(3S_1-1P_1)} \right. \\
& -0.23 g_{(\Delta I=0)}^{(1S_0-3P_0)} \\
& +0.15 g_{(\Delta I=1)}^{(1S_0-3P_0)} \\
& \left. -1.08 g^{(3S_1-3P_1)} \right] \times 10^3.
\end{aligned} \tag{15}$$

2. Photon asymmetries in $nd \rightarrow {}^3H\gamma$

In the three-body system, other PV observables are the asymmetries of the γ -emission. The equation

$$\frac{1}{\Gamma} \frac{d\Gamma}{d \cos\theta} = 1 + O_\gamma \cos\theta \tag{16}$$

represents the relation that gives us the asymmetry of photon. In Eq.(16) O_γ represents e.g. a_γ^{nd} (A_γ^{nd}) which is the asymmetry of the outgoing photon with respect to the neutron (deuteron) polarization in $nd \rightarrow {}^3H\gamma$. Γ is the process width and θ denotes the angle between neutron (deuteron) polarization and outgoing photon direction. By using Eq.(16), we can see that a_γ^{nd} and A_γ^{nd} are given in terms of the PC and PV amplitudes of $nd \rightarrow {}^3H\gamma$ by,

$$\begin{aligned}
a_\gamma^{nd} = & \frac{2}{3} Re \left[\sqrt{2} \mathcal{W}^{PC\dagger}(2S_{\frac{1}{2}}) \mathcal{W}^{PV}(4S_{\frac{3}{2}}) + \sqrt{2} \mathcal{W}^{PC\dagger}(4S_{\frac{3}{2}}) \mathcal{W}^{PV}(2S_{\frac{1}{2}}) \right. \\
& \left. + \frac{5}{2} \mathcal{W}^{PC\dagger}(4S_{\frac{3}{2}}) \mathcal{W}^{PV}(4S_{\frac{3}{2}}) - \mathcal{W}^{PC\dagger}(2S_{\frac{1}{2}}) \mathcal{W}^{PV}(2S_{\frac{1}{2}}) \right] \\
& / \left[|\mathcal{W}^{PC}(2S_{\frac{1}{2}})|^2 + |\mathcal{W}^{PC}(4S_{\frac{3}{2}})|^2 \right],
\end{aligned} \tag{17}$$

and

$$\begin{aligned}
A_\gamma^{nd} = & -Re \left[\sqrt{2} \mathcal{W}^{PC\dagger}(2S_{\frac{1}{2}}) \mathcal{W}^{PV}(4S_{\frac{3}{2}}) + \sqrt{2} \mathcal{W}^{PC\dagger}(4S_{\frac{3}{2}}) \mathcal{W}^{PV}(2S_{\frac{1}{2}}) \right. \\
& \left. - 5 \mathcal{W}^{PC\dagger}(4S_{\frac{3}{2}}) \mathcal{W}^{PV}(4S_{\frac{3}{2}}) - 4 \mathcal{W}^{PC\dagger}(2S_{\frac{1}{2}}) \mathcal{W}^{PV}(2S_{\frac{1}{2}}) \right] \\
& / \left[|\mathcal{W}^{PC}(2S_{\frac{1}{2}})|^2 + |\mathcal{W}^{PC}(4S_{\frac{3}{2}})|^2 \right].
\end{aligned} \tag{18}$$

From Eqs.(17) and (18) and the results of PC and PV amplitudes of $nd \rightarrow {}^3H\gamma$, we obtain

$$\begin{aligned}
a_\gamma^{nd} = & \left[-0.51 g^{({}^3S_1-{}^1P_1)} \right. \\
& +0.83 g_{(\Delta I=0)}^{({}^1S_0-{}^3P_0)} \\
& -0.47 g_{(\Delta I=1)}^{({}^1S_0-{}^3P_0)} \\
& \left. +1.36 g^{({}^3S_1-{}^3P_1)} \right] \times 10^3, \tag{19}
\end{aligned}$$

$$\begin{aligned}
A_\gamma^{nd} = & \left[1.36 g^{({}^3S_1-{}^1P_1)} \right. \\
& -1.50 g_{(\Delta I=0)}^{({}^1S_0-{}^3P_0)} \\
& +0.94 g_{(\Delta I=1)}^{({}^1S_0-{}^3P_0)} \\
& \left. -4.47 g^{({}^3S_1-{}^3P_1)} \right] \times 10^3. \tag{20}
\end{aligned}$$

We note that the contributions of the diagrams in Figs.1 and 2 are calculated with the same cutoff value, $\Lambda = 700$ MeV. The evaluation of the photon asymmetries in $nd \rightarrow {}^3H\gamma$ will be carried out in Sect.V, however primarily, we need to obtain the value of the PV LECs in the next section.

IV. THE DETERMINATION OF THE PARITY-VIOLATING LOW-ENERGY COUPLING CONSTANTS

The EFT(\not{t}) predicted relations for PV observables with the capability of power counting provide a reliable calculation with controlled theoretical errors. Therefore, the PV observables can be introduced in terms of five PV LECs according to the formalism based on EFT(\not{t}) framework. However, the lack of experimental values for the PV observables are the main obstacle so far to determine the PV LECs.

At the present circumstances, we intend to match the EFT(\not{t}) calculated relations for the PV observables with the DDH estimates in order to obtain the PV LECs.

The EFT(\not{t}) relations for A_γ^{np} and P_γ^{np} observables at LO are [5]

$$A_\gamma^{np} = 2m_N^2 \sqrt{\frac{\rho_d}{\pi}} \frac{1 - \frac{\gamma_t a_t}{3}}{k_1(1 - \gamma_t a_s)} g^{({}^3S_1-{}^3P_1)}, \tag{21}$$

and

$$P_\gamma^{np} = -2 \sqrt{\frac{\rho_d}{\pi}} \frac{m_N^2}{k_1(1 - \gamma_t a_s)} \left[\left(1 - \frac{2}{3} \gamma_t a_s\right) g^{({}^3S_1-{}^1P_1)} + \frac{\gamma_t a_s}{3} \sqrt{\frac{r_0}{\rho_d}} \left(g_{(\Delta I=0)}^{({}^1S_0-{}^3P_0)} - 2 g_{(\Delta I=2)}^{({}^1S_0-{}^3P_0)} \right) \right], \tag{22}$$

TABLE III: The theoretical values of five PV observables which are used in the determination of the PV LECs.

PV observable	Model used for matching	Value
P_γ^{np} [15]	AV18+DDH-II	1.76×10^{-8}
A_γ^{np} [15]	AV18+DDH-II	5.29×10^{-8}
$\frac{d\phi^{np}}{dl}$ [6]	DDH-best	$3.2 \times 10^{-17} \text{ rad.fm}^{-1}$
$\frac{d\phi^{nd}}{dl}$ [16]	AV18+UIX/DDH-best	$9.32 \times 10^{-17} \text{ rad.fm}^{-1}$
P_γ^{nd} [15]	AV18+UIX/DDH-II	-7.30×10^{-7}

where a_t is the NN scattering length in 3S_1 channel. r_0 and ρ_d denote the effective ranges in singlet and triplet NN channels, respectively. We use the nucleon mass $m_N = 938.918$ MeV, the isovector nucleon magnetic moment $k_1 = 2.35294$, deuteron binding momentum $\gamma_t = 45.7025$ MeV, effective range of NN singlet (triplet) channel $r_0 = 2.73$ fm ($\rho_d = 1.764$ fm) and scattering length in the singlet (triplet) channel $a_s = -23.714$ fm ($a_t = \frac{1}{\gamma_t}$), so we have

$$A_\gamma^{np} = \left(4.102 g^{(^3S_1-^3P_1)}\right) \times 10^3, \quad (23)$$

$$P_\gamma^{np} = \left(-28.699 g^{(^3S_1-^1P_1)} + 14.024 [g_{(\Delta I=0)}^{(^1S_0-^3P_0)} - 2g_{(\Delta I=2)}^{(^1S_0-^3P_0)}]\right) \times 10^3, \quad (24)$$

The EFT(\not{t}) results of np and nd spin rotations in terms of the PV coupling constants at NLO are [6],

$$\frac{1}{\rho} \frac{d\phi^{np}}{dl} = \left(4.5 [2g^{(^3S_1-^3P_1)} + g^{(^3S_1-^1P_1)}] - 18.5 [g_{(\Delta I=0)}^{(^1S_0-^3P_0)} - 2g_{(\Delta I=2)}^{(^1S_0-^3P_0)}]\right) \text{ rad.MeV}^{-2}, \quad (25)$$

and

$$\frac{1}{\rho} \frac{d\phi^{nd}}{dl} = \left(8.0 g^{(^3S_1-^3P_1)} + 17.0 g^{(^3S_1-^1P_1)} + 2.3 [3g_{(\Delta I=0)}^{(^1S_0-^3P_0)} - 2g_{(\Delta I=1)}^{(^1S_0-^3P_0)}]\right) \text{ rad.MeV}^{-2}, \quad (26)$$

where $\rho = 0.04 \text{ fm}^{-3}$ is the target density.

From Eqs.(15) and (23-26), we have five relations which are sufficient for the determination of five PV unknown coupling constants. For obtaining the PV coupling constants, we use the results of PV observables based on the DDH method presented in Table III.

TABLE IV: Results of the obtained PV LECs in $\text{MeV}^{-\frac{3}{2}}$ unit. Our outcomes are obtained using the results of P_γ^{np} , A_γ^{np} , $\frac{d\phi^{np}}{dl}$, $\frac{d\phi^{nd}}{dl}$ and P_γ^{nd} observables which are introduced in Table III.

$g(^3S_1-^1P_1)$	$g(^1S_0-^3P_0)_{(\Delta I=0)}$	$g(^1S_0-^3P_0)_{(\Delta I=1)}$	$g(^1S_0-^3P_0)_{(\Delta I=2)}$	$g(^3S_1-^3P_1)$
2.78×10^{-12}	4.71×10^{-9}	2.41×10^{-9}	2.35×10^{-9}	1.29×10^{-11}

TABLE V: Comparison between different theoretical results for photon asymmetries in $nd \rightarrow ^3H\gamma$ process. The row 9 shows our EFT($\not{\mathcal{A}}$) results at LO. Our results in row 9 are obtained using the determined values of the PV LECs which are presented in Table IV.

Method	a_γ^{nd}	A_γ^{nd}
DDH(RSC potential) [17]	0.61×10^{-6}	-1.40×10^{-6}
DDH(SSC potential) [17]	0.81×10^{-6}	-1.60×10^{-6}
DDH best values(AV18+UIX/DDH-I) [15]	3.30×10^{-7}	-8.23×10^{-7}
DDH best values(AV18+UIX/DDH-II) [15]	4.11×10^{-7}	-9.04×10^{-7}
DDH best values(NijmII/DDH-II) [15]	4.71×10^{-7}	-1.05×10^{-6}
4-parameter fits(AV18+UIX/DDH-I) [15]	1.97×10^{-7}	-1.81×10^{-7}
4-parameter fits(AV18+UIX/DDH-II) [15]	4.14×10^{-7}	-4.09×10^{-7}
4-parameter fits(NijmII/DDH-II) [15]	4.76×10^{-7}	-4.41×10^{-7}
our EFT($\not{\mathcal{A}}$)	2.82×10^{-6}	-4.87×10^{-6}
Experiment [18]	$(4.2 \pm 3.8) \times 10^{-6}$	-

Our obtained results for $g^{(\bar{X}-\bar{Y})}$ are shown in Table IV. Our outcomes in Table IV are obtained using the results in Table III for P_γ^{np} , A_γ^{np} , $\frac{d\phi^{np}}{dl}$, $\frac{d\phi^{nd}}{dl}$ and P_γ^{nd} observables. In the next section, we evaluate the a_γ^{nd} and A_γ^{nd} using the values of $g^{(\bar{X}-\bar{Y})}$.

V. THE RESULT OF PHOTON ASYMMETRIES IN $nd \rightarrow ^3H\gamma$ PROCESS

From Table IV and Eqs.(19) and (20), we can extract the values of the a_γ^{nd} and A_γ^{nd} . We compare our EFT results of a_γ^{nd} and A_γ^{nd} with the previous theoretical calculations based on the DDH model and the available experimental data in Table V. Our EFT($\not{\mathcal{A}}$) results in row

9 of Table V are evaluated using the outcomes shown in Table IV.

The sign and the order of a_γ^{nd} results are rightly comparable with the only available experimental data. There is no experimental data for A_γ^{nd} , however, the results are in the expected limits.

VI. CONCLUSION AND OUTLOOK

In this paper, we have incorporated five relations for PV observables in terms of PV LECs in the EFT(π) framework. We obtain the PV LECs by matching these five relations onto the corresponding results for PV observables which are calculated based on the different DDH PV potential combinations.

The extraction of the results for a_γ^{nd} and A_γ^{nd} have been done using the relationship between corresponding observables and the PV low-energy coupling constants.

The asymmetries from $\vec{\gamma}^3H \rightarrow nd$ or $\vec{\gamma}^3He \rightarrow pd$ and the longitudinal asymmetry in $\vec{p}d$ scattering are the other theoretical analyses which could be studied in the EFT(π) framework using the determined PV LECs.

The model independent EFT(π) predictions for observables and particularly PV observables in terms of PV LECs require principally to be fixed by experimental data. However, this task does not look feasible in the nearest future.

Acknowledgments

This work was supported by the research council of the University of Tehran.

Appendix. INTRODUCTION OF THE DIAGRAMS USED IN THE TEXT

The PC Nd scattering amplitude is used for calculating the PC and PV amplitudes of $nd \rightarrow {}^3H\gamma$ process. In Figs.1 and 2, the PC amplitude of Nd scattering at LO is introduced by the dashed oval. The Faddeev equation that calculates the PC Nd scattering amplitude is schematically shown in Fig.3. The detail calculation process for solving this Faddeev equation in an arbitrary channel in the cluster-configuration space is previously reported in [13]. We emphasize that the normalized triton wave function, which is introduced in the text

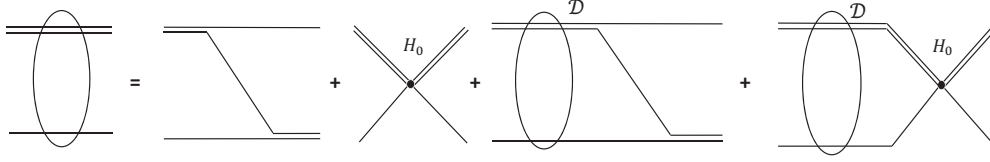


FIG. 3: The Faddeev equation for the Nd scattering at the leading order. All notations are the same as the previous figures.

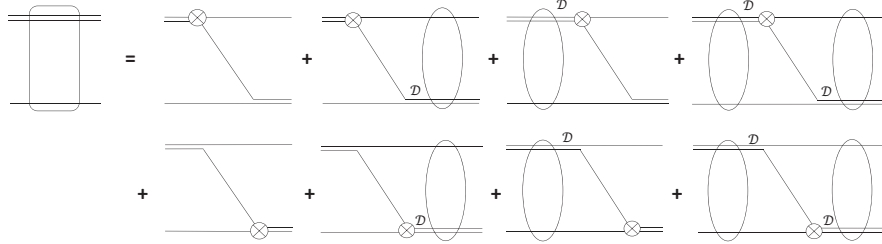


FIG. 4: The PV Nd scattering diagrams at LO. The dashed rectangular denotes the PV Nd scattering amplitude. Circle with a cross indicates the PV dNN vertex. Remaining notations are the same as the previous figures.

with the dashed half-oval, is obtained by solving the homogeneous part of Faddeev equation of the PC Nd scattering [7].

In the text, Fig.2 shows the diagrams which participate in the PV amplitude of $nd \rightarrow {}^3H\gamma$ process. The diagrams making the dashed rectangular and the box with the wavy line of Fig.2 are introduced in Figs.4 and 5, respectively. In Fig.5, the dashed rectangular with the dashed line around it is the sum of the PV Nd scattering diagrams which have no PC Nd scattering in the right hand side. The last line of Fig.5 shows these diagrams.

-
- [1] Danilov G S (1965) Phys Lett 18:40.
 - [2] Desplanques B, Missimer J (1978) Nucl Phys A 300:286.
 - [3] Desplanques B, Donoghue J F, Holstein B R (1980) Annals Phys 124:449.
 - [4] Schindler M R, Springer R P (2013) Prog Part Nucl Phys 72:1.
 - [5] Schindler M R, Springer R P (2010) Nucl Phys A 846:51. [arXiv:nucl-th/0907.5358].
 - [6] Grießhammer H W, Schindler M R, Springer R P (2012) Eur Phys J A 48:7.
 - [7] Arani M M, Bayegan S (2013) Euro Phys J A 49:117.

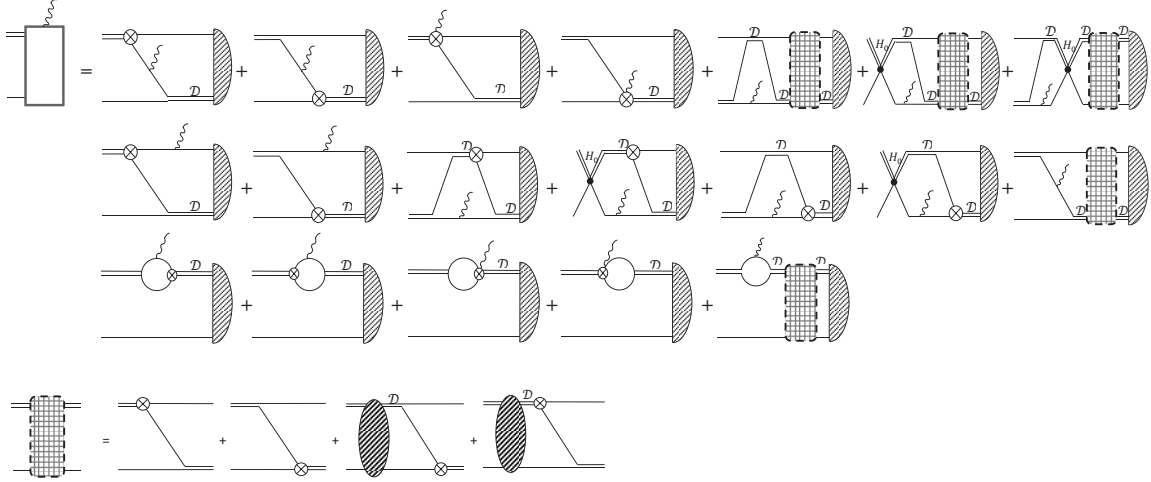


FIG. 5: The box with wavy line which is used in Fig.2. Circle with a cross and wavy line is the PV E1 photon-dibaryon-nucleon-nucleon (γdNN) vertex. The dashed rectangular with dashed line around it is the contribution of the some of the PV Nd scattering diagrams which are introduced in the last line. All notations are the same as the Fig.2.

- [8] Cavaignac J F, Vignon B, Wilson R (1977) Phys Lett B 67:148 .
- [9] Alberi J, et al. (1988) Can J Phys 66:542.
- [10] Snow W M, et al. (2000) Phys Res A 440:729.
- [11] Knyazkov V A, et al. (1984) Nucl Phys A 417:209.
- [12] Phillips D R, Rupak G, Savage M J (2000) Phys Lett B 473:209.
- [13] Griebhammer H W (2004) Nucl Phys A 744:192.
- [14] Griebhammer H W, Schindler M R (2010) Eur Phys J A 46:73. [arXiv:nucl-th/10070734].
- [15] Song Y, Lazauskas R, Gudkov V (2012) Phys Rev C 86:045502. [arxiv:nucl-th/1207.7039v1].
- [16] Schiavilla R, Viviani M, Girlanda L, Kievsky A, Marcucci L E (2008) Phys Rev C 78:014002. (2011)(E) 83:029902.
- [17] Desplanques B, Benayoun J J (1986) Nucl Phys A 458:689.
- [18] Avenier A, et al. (1984) Phys Lett B 137:125.